PAPER *Special Section on Multiple-Valued Logic and VLSI Computing*

Evaluating PAM-4 Data Transmission Quality Using Multi-Dimensional Mapping of Received Symbols

Yasushi YUMINAKA[†a)], ***Senior Member***, **Kazuharu NAKAJIMA**[†], ***Nonmember***, ***and*** **Yosuke IIJIMA**[††], ***Member***

SUMMARY This study investigates a two/three-dimensional (2D/3D) symbol-mapping technique that evaluates data transmission quality based on a four-level pulse-amplitude modulation (PAM-4) symbol transition. Multi-dimensional symbol transition mapping facilitates the visualization of the degree of interference (ISI). The simulation and experimental results demonstrated that the 2D symbol mapping can evaluate the PAM-4 data transmission quality degraded by ISI and visualize the equalization effect. Furthermore, potential applications of 2D mapping and its extension to 3D mapping were explored.

key words: *multi-valued signaling, pulse-amplitude modulation (PAM-4), intersymbol interference (ISI), eye-opening monitor, multi-dimensional symbol mapping*

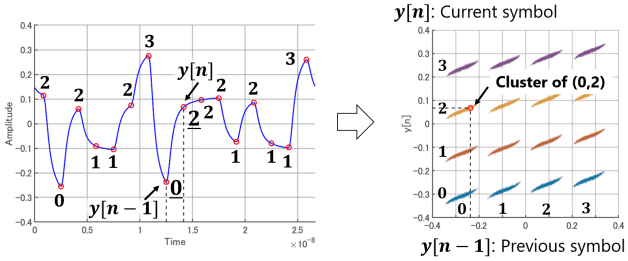

Fig. 1 2D mapping of the PAM-4 received symbols.

1. Introduction

The growing demand for high-speed and high-capacity information and communication services, such as the Internet of Things (IoT), cloud computing, and data centers, has increased data transmission volumes [1]. However, in high-speed wireline communications, the inherent low-pass filter attributes of transmission components, such as boards and cables, introduce intersymbol interference (ISI) and data errors in the received signals. Consequently, adopting the four-level pulse-amplitude modulation (PAM-4) is viable because it facilitates the transmission of two-bit binary data within a single symbol. This multilevel coding technique halves the Nyquist frequency of the transmitted signal compared to that of the binary signal at the same data rate. Consequently, PAM-4 coding can mitigate the waveform degradation attributed to the bandwidth limitations of transmission lines.

However, owing to the proximity between symbols, PAM-4 signaling is three times more sensitive to the noise amplitude than binary signaling. This heightened sensitivity complicates the threshold discrimination and accurate identification of four-level symbols. To mitigate this issue, continuous-time linear equalizers (CTLEs) and decision feedback equalizers (DFEs) are employed to counteract ISI at the receiver end [2], [3]. Waveform-shaping circuits require parameter adjustments based on the transmission line characteristics. Therefore, eye diagrams are used to evaluate the ISI degree on the degraded waveform at the receiving end [4], [5].

However, extracting information regarding the extent of degradation and transmission line conditions from eye diagrams becomes challenging under stringent bandwidth limitations and conditions wherein the eye diagram is closed. To address this issue, a PAM-4 data transmission quality evaluation method based on the Gaussian mixture model is proposed [6]–[9]. Additionally, a novel two-dimensional (2D) mapping method is proposed to evaluate the degraded symbol distribution using an analog-to-digital converter at the receiving end [10]–[13]. Figure 1 shows that the 2D symbol mapping represents the received data on a 2D plane with the current and previous symbols on the y- and x-axis, respectively. Such 2D mapping visualizes the ISI effect after transmission through lines and evaluates the PAM-4 data transmission quality.

This study investigated the properties of the 2D mapping used for PAM-4 data transmission quality evaluation. The simulation and experimental results of 2D mapping show the visualization effects of the equalization and nonlinearity of the transmitter. Furthermore, this method is extended to 3D mapping, which visualizes the effect of the symbol that precedes and succeeds the received symbol.

Section 2 describes the method for generating 2D mapping. Section 3 discusses its properties and applications, such as visualizing the effect of waveform equalization and nonlinearity of a transmitter. Section 4 presents the simulation and experimental results, confirming the validity and feasibility of the proposed 2D mapping. Section 5 extends this to 3D mapping based on the time-domain information and other factors. Finally, Sect. 6 presents the conclusions.

2. 2D Mapping Using PAM-4 Symbol Transition

Our previous study introduced a novel approach for assessing

Manuscript received October 22, 2023.
Manuscript revised March 3, 2024.
Manuscript publicized April 25, 2024.

[†]Graduate School of Science and Technology, Gunma University, Kiryu-shi, 376–8515 Japan.
[††]National Institute of Technology (KOSEN), Oyama College, Oyama-shi, 323–0806 Japan.
a) E-mail: yuminaka@gunma-u.ac.jp

DOI: 10.1587/transinf.2023LOP0004

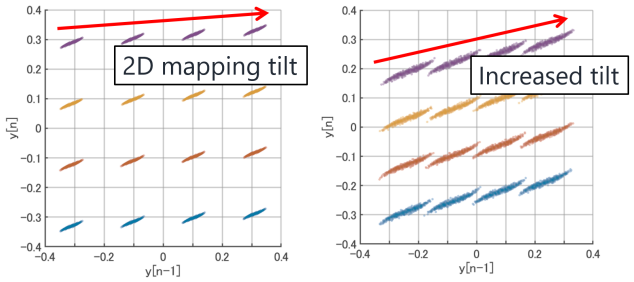

(a) 0.6 Gb/s PAM-4 signaling (b) 1.8 Gb/s PAM-4 signaling

Fig. 2 Variation in the point-cloud distribution of 2D mapping by symbol rate.

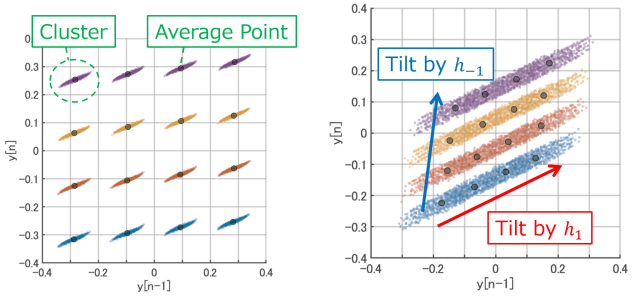

(a) 1 Gb/s PAM-4 signaling (b) 4 Gb/s PAM-4 signaling

Fig. 3 Relationship between the distribution of symbol clusters and the impulse response coefficients for 2D mapping.

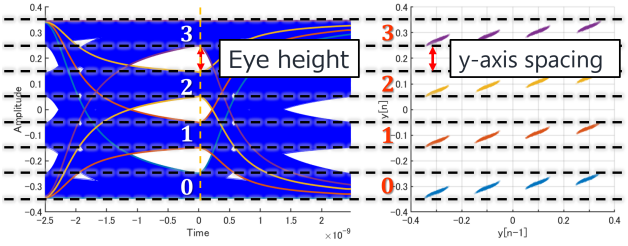

Fig. 4 Relationship between the eye diagram and the 2D mapping.

data transmission quality [12]–[14], which involved using a 2D PAM-4 symbol transition mapping method. Based on this, the PAM-4 symbols $(\ldots, y[n-1], y[n], y[n+1], \ldots)$ were represented on a 2D plane, with the x- and y-axis corresponding to the previous ($y[n-1]$) and current ($y[n]$) symbol values, respectively, as shown in Fig. 1. This mapping illustrates the behavior of 16 ($= 4 \times 4$) distinct data transition patterns of PAM-4 symbols $(0, 1, 2, 3)$ within the 2D plane. In an ideal PAM-4 signal transmission scenario devoid of ISI and attenuation along the transmission line, the symbols are aligned in a perfect grid pattern comprising 16 points.

Figure 2 shows the point-cloud distribution for a 2D mapping as the PAM-4 symbol rate varied from 0.6 to 1.8 Gb/s. With an increased symbol rate, the sampled values diverged from their ideal values owing to ISI, which caused significant variability within each point cloud in the 2D mapping and tilted the point-cloud orientation. The data for these 2D mapping were obtained using MATLAB simulation. Then, 2D mapping is evaluated through simulation. In the simulation, the S-parameters obtained from a 2-m long microstrip line (MSL) for evaluation were used as the transmission line model.

The point-cloud tilt can be mathematically described based on the relationship among the impulse responses of the transmission line. Let $a[n]$ and $y[n]$ represent the transmitted and received symbol values, respectively. The following first-order approximation expresses their relationship [13]:

$$\begin{aligned} y[n-1] &\simeq h_0 a[n-1] + h_{-1} a[n] \\ y[n] &\simeq h_1 a[n-1] + h_0 a[n], \end{aligned} \tag{1}$$

where h_{-1}, h_0, and h_1 correspond to the *pre*-cursor, *main*-cursor, and *post*-cursor, respectively. The term $h_{-1}a[n]$ indicates that increasing the value of $a[n]$ increases that of $y[n-1]$. Similarly, the term $h_1 a[n-1]$ indicates that $a[n-1]$ increases as $y[n]$ increases.

Figure 3 shows the simulation results of the relationship in a 2D map containing 16-point clusters corresponding to the transmitted symbols whose averages are denoted by points. Therefore, the aforementioned relationship skews the cluster order in the 2D mapping, i.e., h_1 and h_{-1} skew the 2D mapping (Fig. 3 (b)). Furthermore, the scatter and tilt of the 2D-mapping point cloud increases with increasing data rate. Here, the data width of the diagonal line is related to the symbol error rate because it spreads due to the effects of jitter and inter-symbol interference.

Additionally, an interesting mirror effect is noted where the spacing of the point clouds is similar regardless of whether they are viewed from above or the right.

3. Properties of 2D Mapping

This section discusses the properties of the proposed 2D mapping method, particularly the eye-diagram aperture. Subsequently, the visualization capabilities of the 2D mapping were demonstrated by shaping the waveform using the equalization circuit and nonlinearity in the transmitter driver.

3.1 Relationship between the Eye Diagram and 2D Mapping

Figure 4 shows the simulation results of the relationship between the proposed 2D mapping and eye diagram – a prevalent metric for evaluating high-speed signal transmission quality [12], [13]. The vertical spacing between the point clouds in the 2D mapping corresponds to the amplitude of the height of each eye at the sampling point within the PAM-4 eye diagram.

Increased data rates resulted in a steeper slope of the point cloud and reduced the spacing between the point clouds along the y-axis. Consequently, the y-axis spacing in the 2D mapping became more compressed, thereby closing the eye diagram.

The 2D mapping can also be applied to PAM-8 signaling, representing 64 ($= 8 \times 8$) distinct symbol transitions.

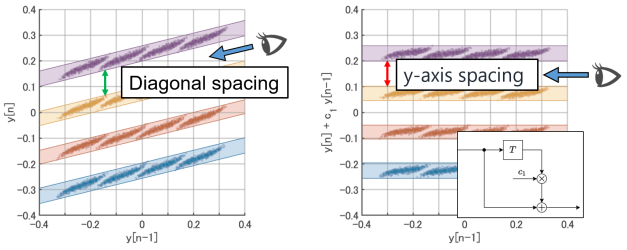

(a) Before correction (b) Correction by rotation

Fig. 5 Correlation between the 2D mapping tilt adjustment and the FFE functionality.

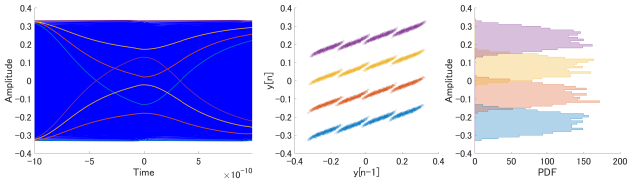

(a) 2 Gb/s PAM-4 signaling without FFE

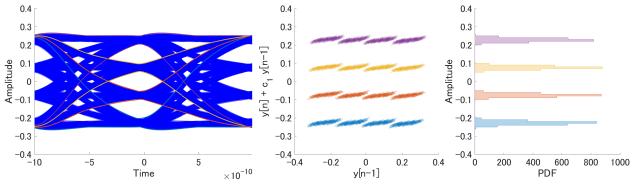

(b) 2 Gb/s PAM-4 signaling with FFE

Fig. 6 Visualization of the equalizer effect (first-order equalization is a sufficient condition).

The PAM-8 eye diagram exhibits compact symbol spacing, challenging the extraction of details, such as intersymbol transitions. Alternatively, the 2D mapping reveals the detailed ISI characteristics of the transmission line for PAM-8 signaling, even when the eye remains entirely closed.

3.2 Visualization of the Feed-Forward Equalizer Operation

The diagonal view of the point cloud reveals an opening under conditions that condense the y-axis spacing, as shown in Fig. 5 (a). Herein, the tilt of the mapping axes can be adjusted, transforming the diagonal spacing into y-axis spacing, as shown in Fig. 5 (b). This adjustment was assumed to enhance the eye diagram clarity.

The y-axis was transformed from $y[n]$ to $y[n]+c_1 y[n-1]$. In particular, by adjusting the 2D mapping, the value of the prior symbol was multiplied by c_1 and summed with the value of the current symbol. This procedure corresponds to the operation of a first-order feed forward equalizer (FFE) [2], [15], [16], as shown in Fig. 5 (b).

Figure 6 shows the simulation results, where an FFE operation was performed on the 2 Gb/s PAM-4 waveforms degraded by a 2 m-long MSL, exhibiting an attenuation of 1 GHz at -16.6 dB.

Implementing FFE rectifies the 2D mapping skewness, thereby expanding the point-cloud spacing along the y-axis. This adjustment is analogous to the operation of opening

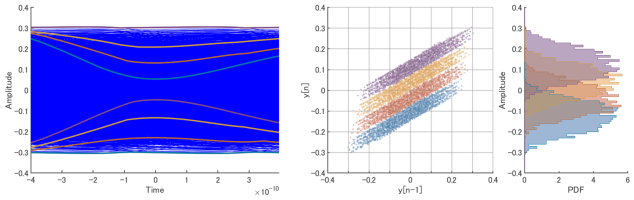

(a) 5 Gb/s PAM-4 signaling without FFE

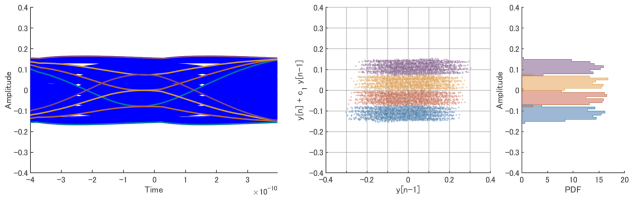

(b) 5 Gb/s PAM-4 signaling with FFE

Fig. 7 Visualization of the equalizer effect (first-order equalization is an insufficient condition).

the eye. On the right-hand side, the probability distribution function (PDF) plot was derived by projecting the symbol distributions onto the y-axis. Distribution curves for each symbol were constructed by integrating four Gaussian distributions. The condition for eye-opening was achieved when these curves did not overlap.

The results indicate that the FFE effects can be visualized using 2D mapping. Figure 7 shows the simulation results under transmission conditions, where the symbol rate increases and the distance of the point clouds from the diagonal decreases. Under these conditions, the spacing between the 2D mapping points reduces even when observed from a diagonal angle. Consequently, the eye remained closed despite the first-order FFE compensating for the tilt. Thus, the 2D mapping depicts whether the first-order FFE can compensate for the degraded waveform, revealing the limits of transmission conditions.

3.3 Visualization of Transmitter Nonlinearity

A fundamental requirement for PAM-4 signaling is achieving equally spaced amplitude levels across all four symbol levels. Compared with binary signaling, the design of a PAM-4 transmitter imposes stringent linearity constraints. The amplitude distortion should be minimized to maintain a constant signal-to-noise ratio (SNR) within the three eyes. This distortion is attributed to nonlinearity issues, such as compression and expansion in the driver amplifiers at the transmitter [4].

The 2D mapping depicts the nonlinear effects on the transmitter driver. Operating this driver at elevated speeds increases the complexity of maintaining the optimal voltage values for the transmitted symbols close to the supply voltage, as shown in Fig. 8 (a). This nonlinearity causes irregular spacing between eye diagram symbols, as shown in Fig. 8 (b). In a related 2D visualization, the transitions between symbols manifest as asymmetric point clouds.

Figure 8 (c) shows the closed-eye diagram and the cor-

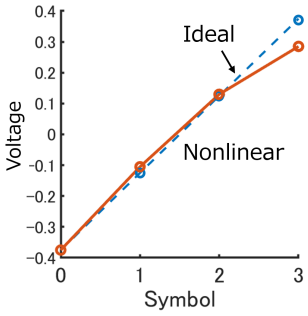

(a) Relationship between symbol and voltage

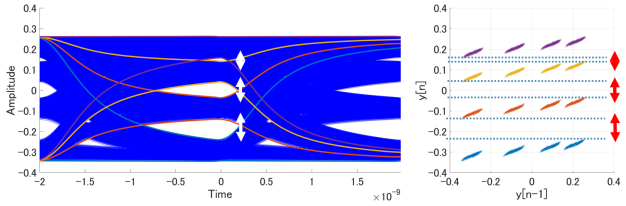

(b) Eye diagram and corresponding 2D mapping

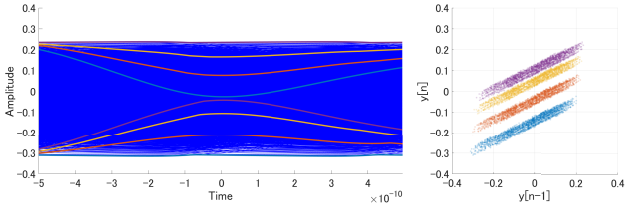

(c) Closed eye diagram and corresponding 2D mapping

Fig. 8 Visualization of transmitter nonlinearity using 2D mapping.

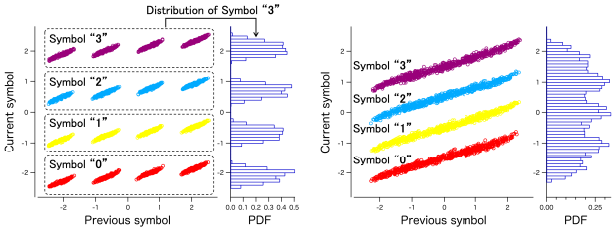

(a) 1 Gbps PAM-4. (b) 2.5 Gbps PAM-4.

Fig. 9 Simulation results of the 2D mapping and histogram of PAM-4 received symbols with ISI on 2 m-long MSL.

responding 2D mapping simulation results for a severely band-limited transmission line. Driver nonlinearity, which cannot be obtained from a fully closed-eye diagram, can be visualized and evaluated based on the nonuniform spacing between the 2D mapping points.

4. Simulation and Experimental Results of 2D Mapping

This section demonstrates the efficacy of 2D mapping through simulation results and measurement instances.

Figure 9 illustrates the simulation outcomes, including the 2D mapping and PDF histogram, for the received PAM-4 symbols over a 2 m-long MSL environment. Figure 9 (a) shows that during a low ISI impact at 1 Gbps PAM-4, each symbol is individually arranged in the 2D mapping, resulting in separate histograms, as shown in Fig. 9 (a). The PDF

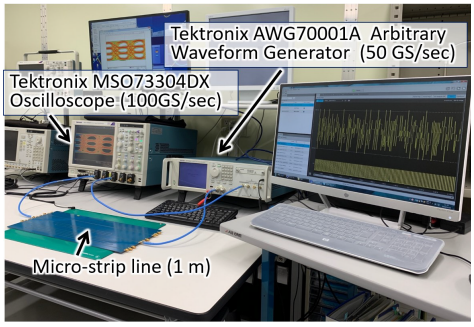

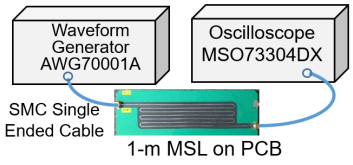

Fig. 10 Experimental setup.

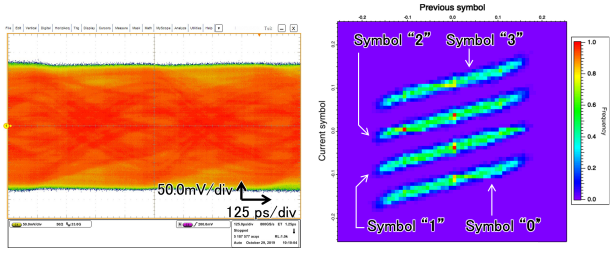

(a) Eye diagram (b) 2D symbol mapping

Fig. 11 Experimental result of 2D symbol mapping using that of the received symbol at 4 Gbps PAM-4 on the 1 m-long MSL.

histogram of symbol **3** represents the cumulative mapping of the distribution of the associated point clouds along the y-axis.

As the data rate escalated to 2.5 Gbps, the point clouds increased owing to the heightened ISI and overlapping distributions of the current symbols, as shown in Fig. 9 (b). Contrastingly, the results at 1 Gbps PAM-4 show that the inclination of each distribution became more pronounced. Consequently, the histogram representing the received symbol projection on the y-axis converged to a single cluster. Figure 9 (b) shows that while 2D symbol mapping effectively visualizes the ISI effect on each symbol transition, the symbol classification encounters challenges while implementing 1D representation, such as a histogram, as shown in Fig. 9 (b).

The experimental configuration for acquiring the PAM-4 sampling signals, which employs an arbitrary waveform generator and oscilloscope, is depicted in Fig. 10. Figure 11 shows the experimental result of a 4 Gbps PAM-4 signal measurement over a 1-m long MSL, showcasing an eye diagram and 2D symbol mapping. The heat map distribution originated from a dataset comprising 3,999,994 sampling points at the receiver. Despite the occlusion in the eye diagram resulting from the superimposed symbols on the y-axis, the 2D

symbol mapping delineated the distribution of each symbol, as shown in Fig. 11 (b). Analyzing the distribution of the received symbols and identifying overlaps using a 1D histogram posed challenges, whereas the 2D mapping approach distinguished each symbol effectively.

This study theoretically verified the 2D mapping characteristics using MATLAB simulations. In particular, depicting the mapping at the sampling point with the largest eye aperture was possible. When the 2D mapping of the received signal is actually realized, the synchronous clock signal can be extracted from the transmitted signal by a clock and data recovery (CDR) circuit, and the sampling timing can be adjusted. However, timing deviations due to jitter, for example, are challenging to adjust even with CDR. This deviation disperses the 2D mapping point cloud; thus, verification of these limitations is a future task.

5. Extension to 3D Mapping

The 2D mapping provides insight into the effect of the *post*-cursor on ISI achieved using the information from the current symbol value $y[n]$ and its immediate predecessor $y[n-1]$ in the received data sequence. Based on this framework, a 3D mapping approach was proposed based on the values of $y[n-1]$, $y[n]$, and $y[n+1]$. The approach considers the symbols that precede and succeed the current symbol, resulting in a representation encompassing three symbols.

Figure 12 (a) shows that the 3D mapping comprehensively represents the 64 ($= 4 \times 4 \times 4$) distinct pattern transitions within the received PAM-4 signal, forming a cubic spatial visualization. This representation captures the effect of the ISI *pre*-cursor – a factor not expressed in the 2D mapping.

The information regarding each symbol transition can be obtained from various orientations within the six planes (top, bottom, and sides); however, the relative planes have identical information. Consequently, three distinct symbol transition distributions, i.e., $(y[n-1], y[n])$, $(y[n+1], y[n])$, and $(y[n-1], y[n+1])$ planes, are derived, as shown in Figs. 12 (b)–(d).

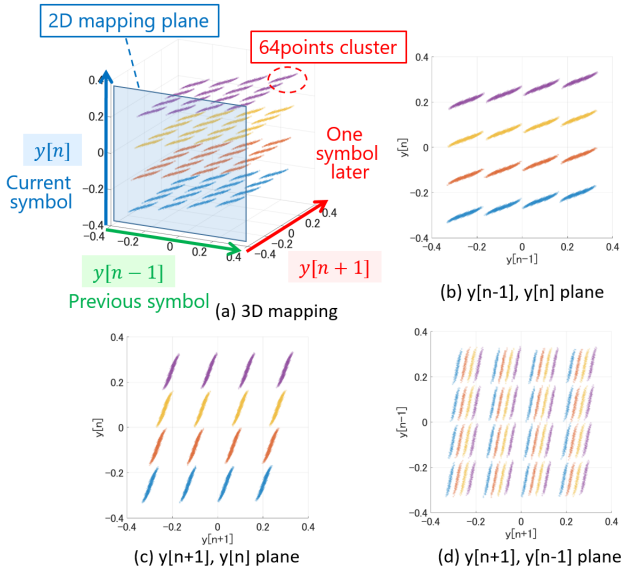

Fig. 12 Simulation results of 3D mapping and views from various planes.

5.1 Second-Order FFE Effect Visualization Using 3D Mapping

Tilt compensation was achieved for 3D mapping analogous to its 2D counterpart. In a 3D context, tilt correction is equivalent to a second-order FFE operation. Figure 13 shows the simulation results of employing the second-order FFE for 5 Gb/s PAM-4 signaling. This scenario mirrors that illustrated in Fig. 7, wherein a first-order FFE fails to recover the symbol adequately. The $(y[n-1], y[n])$ plane is flattened and corrected using the first-order FFE; however, the $(y[n+1], y[n])$ plane has a slope.

The eye diagram in Fig. 13 (b) shows that using a second-order FFE opens the eye. The 3D mapping under this condition represents a scenario wherein the dispersion of the symbol point cloud is discernible from any azimuthal angle when observed orthogonally to the cubic representation. For this instance, the y-axis transformation is defined as $y[n] \rightarrow y[n]+c_1 y[n-1]+c_{-1} y[n+1]$, which is equivalent to the second-order FFE formula.

Additionally, generalized mapping is required to consider a broader range of ISI, such as $y[n-2]$, $y[n-1]$, $y[n]$, $y[n+1]$, and $y[n+2]$, where the ISI is affected by more than ±2 symbols. Nevertheless, visualizing mappings beyond 4D becomes challenging. For the visualization of the effects considering more than ±2 symbols, a scatter plot matrix rather than 2D/3D mapping should be plotted.

5.2 3D Mapping Based on Time-Domain Information

A visualization approach incorporating time-domain infor-

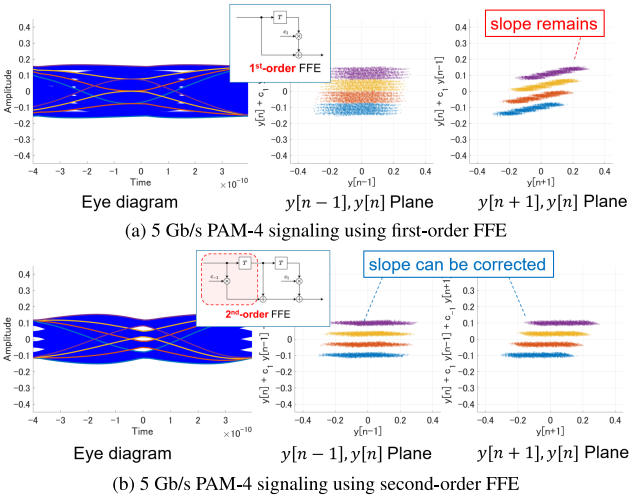

Fig. 13 Visualization of the waveform-shaping effect of the second-order FFE by 3D mapping.

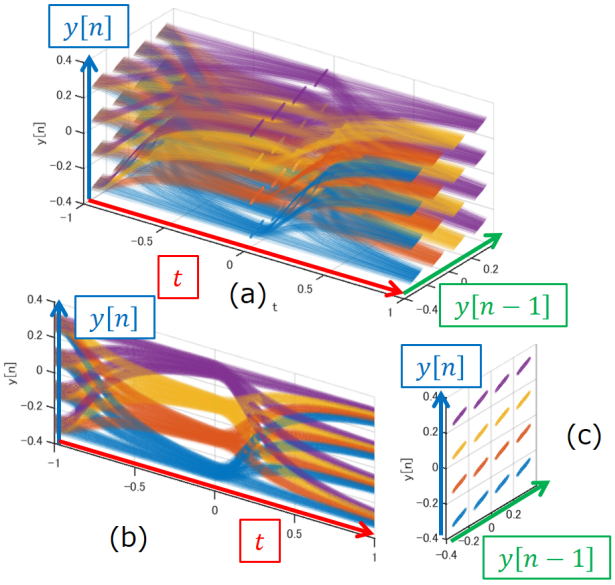

Fig. 14 Simulation results of 3D mapping including time-domain information.

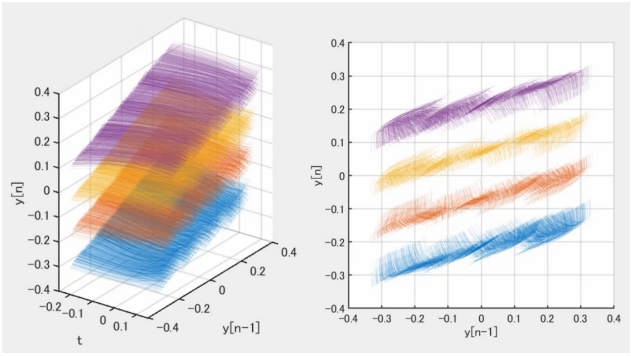

Fig. 15 Temporal superimposition of 2D mapping simulation results within a restricted time range.

mation into a 2D plot was introduced as an additional example of 3D mapping. The 2D plot represents a single sampling point, the maximal eye-opening point, and consequently excludes any temporal information. By modifying the sampling points used for 2D mapping, the plot can be extended along the time axis, creating a 3D map, as shown in Fig. 14 (a). This facilitates the visualization of the temporal evolution of each symbol transition, enabling the detailed observation of time-domain characteristics, such as jitter, induced by transmission lines.

In the 3D mapping of Fig. 14 (a), the plane defined by $(y[n], y[n-1])$ in Fig. 14 (c) represents the symbol transition data analogous to the aforementioned 2D mapping. When projected on the $(t, y[n])$ plane, the resulting graph aligned with a conventional eye diagram, as shown in Fig. 14 (b). Consequently, this 3D representation provides an integrated visualization of the 2D mapping and eye diagram simultaneously, consolidating diverse and pertinent information.

A 3D graph can be derived by restricting the temporal interval of 3D mapping by incorporating time-axis data. When the 3D graph is limited to the interval [-0.2UIto0.15UI] (UI: unit interval) surrounding the sampling point (left panel of Fig. 15), its projection on the $(y[n], y[n-1])$ plane results in the 2D mapping (right panel of Fig. 15). In the 2D plane, the symbol transitions are superimposed within the interval [-0.2UI, 0.15UI] around the sampling points, assessing the open eye in the time domain adjacent to these points.

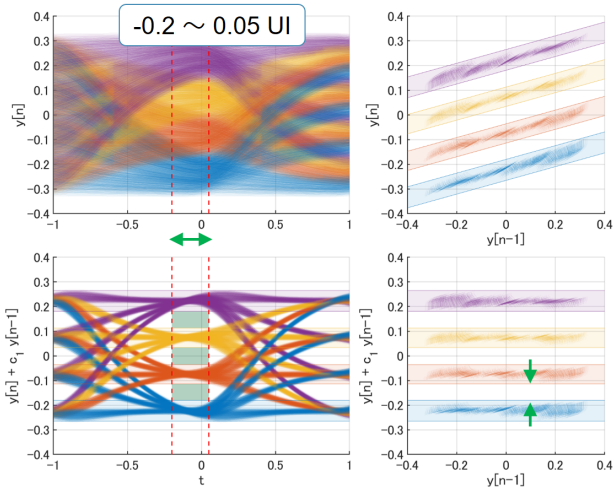

Fig. 16 Simulation results of eye aperture evaluation considering information within a specific time range.

In Fig. 16, the top representation corresponds to the 2D projection showcasing the PAM-4 eye diagram without equalization delineated within the interval [-0.2UI, 0.05UI]. This representation integrates the sampling points discussed in Sect. 3 and superimposes a 2D projection of the symbol transitions preceding and succeeding the sampling instances, providing insights into the temporal dynamics. The effect of sampling timing jitter is discernible in this visualization.

As shown in the lower diagram of Fig. 16, applying FFE to the depicted graph and executing rotation operations verify the operation of opening the eye. This methodology assesses the amplitude direction and time-domain condition for opening the eye. This aligns with the rectangular eye mask test assessment, demonstrating its superior visualization potential for data transmission quality evaluation using 3D mapping.

6. Conclusion

This study proposed a novel PAM-4 data transmission quality evaluation technique for high-speed wireline communications based on the multi-dimensional mapping of received symbols. The MATLAB simulations and experimental results demonstrated that the proposed symbol mapping technique assesses the PAM-4 data transmission quality, particularly when degraded by the ISI of transmission lines. Additionally, this method visually evaluated the efficacy of equalization and the effects of transmitter nonlinearity.

This study is a significant effort in the realm of PAM-4 data transmission quality assessment, highlighting the novel use of 2D and 3D mapping techniques. Future studies may focus on the quantitative evaluation of degradation levels using actual transmission waveforms.

Acknowledgments

This work was supported by JSPS KAKENHI Grant Numbers JP21H01381 and JP21K11819 and the foundation for technology promotion of electronic circuit board.

References

[1] IEEE P802.3bs 200 Gb/s and 400 Gb/s Ethernet Task Force, https://www.ieee802.org/3/bs/
[2] J.R. Barry, E.A. Lee, and D.G. Messerschmitt, Digital Communication, Kluwer Academic Publishers, 2004.
[3] D. Cui, H. Zhang, N. Huang, A. Nazemi, B. Catli, H.G. Rhew, B. Zhang, A. Momtaz, and J. Cao, "A 320mW 32Gb/s 8b ADC-based PAM-4 analog front-end with programmable gain control and analog peaking in 28nm CMOS," 2016 IEEE International Solid-State Circuits Conference (ISSCC), pp.58–59, 2016.
[4] Y. Yuminaka, T. Kitamura, and Y. Iijima, "PAM-4 eye diagram analysis and its monitoring technique for adaptive pre-emphasis for multi-valued data transmissions," IEEE 47th International Symposium on Multiple-Valued Logic, pp.13–18, 2017.
[5] B. Analui, A. Rylyakov, S. Rylov, M. Meghelli, and A. Hajimiri, "A 10-Gb/s two-dimensional eye-opening monitor in 0.13-μm standard CMOS," IEEE J. Solid-State Circuits, vol.40, no.12, pp.2689–2699, 2005.
[6] Y. Yuminaka, K. Taya, and Y. Iijima, "PAM-4 eye-opening monitoring techniques based on Gaussian mixture model fitting," IEICE Communications Express, vol.9, no.10, pp.464–469, 2020.
[7] K. Taya, Y. Yuminaka, and Y. Iijima, "Statistical waveform evaluation method for adaptive PAM-4 equalization," Journal of Applied Logics - IfCoLog Journal of Logics and Their Applications, vol.8, no.4, pp.1087–1099, 2021.
[8] Y. Iijima, K. Taya, and Y. Yuminaka, "PAM-4 eye-opening monitor technique using Gaussian mixture model for adaptive equalization," IEICE Trans. Inf. & Syst., vol.E104-D, no.8, pp.1138–1145, 2021.
[9] Y. Iijima and Y. Yuminaka, "Efficient PAM-4 data transmission with closed eye using symbol distribution estimation," IEEE 51st International Symposium on Multiple-Valued Logic, pp.195–200, 2021.
[10] F. Lu, P.-C. Peng, S. Liu, M. Xu, S. Shen, and G.-K. Chang, "Integration of multivariate Gaussian mixture model for enhanced PAM-4 decoding employing basis expansion," 2018 Optical Fiber Communications Conference and Exposition (OFC), pp.1–3, 2018.
[11] L. Sun, J. Du, J. Liu, B. Chen, K. Xu, B. Liu, C. Lu, and Z. He, "Intelligent 2-dimensional soft decision enabled by k-means clustering for VCSEL-based 112-Gbps PAM-4 and PAM-8 optical interconnection," Journal of Lightwave Technology, vol.37, no.24, pp.6133–6146, 2019.
[12] Y. Iijima, K. Nakajima, and Y. Yuminaka, "Two-dimensional symbol mapping for evaluating multi-valued data transmission quality," IEEE 52nd International Symposium on Multiple-Valued Logic, pp.170–175, 2022.
[13] Y. Yuminaka, K. Nakajima, and Y. Iijima, "PAM-4 data transmission quality evaluation using two- and three-dimensional mapping of received symbols," IEEE 53rd International Symposium on Multiple-Valued Logic, pp.94–98, 2023.
[14] Y. Iijima, K. Nakajima, and Y. Yuminaka, "Evaluation and symbol classification of multi-valued signaling using two-dimensional symbol mapping with linear mixture model," IEEE 53rd International Symposium on Multiple-Valued Logic, pp.99–104, 2023.
[15] G. Steffan, E. Depaoli, E. Monaco, N. Sabatino, W. Audoglio, A.A. Rossi, S. Erba, M. Bassi, and A. Mazzanti, "A 64Gb/s PAM-4 transmitter with 4-Tap FFE and 2.26pJ/b energy efficiency in 28nm CMOS FDSOI," 2017 IEEE International Solid-State Circuits Conference, pp.116–117, 2017.
[16] T.O. Dickson, H.A. Ainspan, and M. Meghelli, "A 1.8pJ/b 56Gb/s PAM-4 transmitter with fractionally spaced FFE in 14nm CMOS," 2017 IEEE International Solid-State Circuits Conference, pp.118–119, 2017.

Yasushi Yuminaka received B.E., M.E., and D.E. degrees in electronic engineering from Tohoku University, Sendai, Japan, in 1990, 1992, and 1995, respectively. He is currently a Professor in the Division of Electronics and Informatics, Graduate School of Science and Technology, Gunma University, Kiryu, Japan. His research interests include the design of multiple-valued integrated circuits, high-speed interfaces for VLSI systems, and new-paradigm computing systems and their applications. Dr. Yuminaka received the IEE Ambrose Fleming Premium Award in 1994, the Niwa Memorial Award in 1995, the Young Engineer Award from the IEICE of Japan in 1995, and the Outstanding Contributed Paper Award at the IEEE International Symposium on Multiple-Valued Logic in 2000 and 2009. He served as a Program Chair for IEEE International Symposium on Multiple-Valued Logic in 2013, 2016, and 2020, and a Symposium Chair for IEEE International Symposium on Multiple-Valued Logic in 2023. He was a Chair (2020–2021) of the IEEE Computer Society Technical Committee on Multiple-Valued Logic. He is senior members of IEEE and IEEJ.

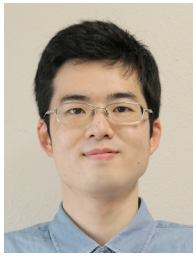

Kazuharu Nakajima received B.E. degree in electronics and informatics from National Institute of Technology, Oyama College, Japan, in 2019, and received M.E. degree in electronic engineering from Gunma University, Kiryu, Japan, in 2023, respectively. His research interests include design of high-speed serial links using multi-valued logic.

Yosuke Iijima received B.E. and M.E. degrees in electronic engineering from Gunma University, Kiryu, Japan, in 2003 and 2005, respectively, and received D.E. degree in electronic engineering from the University of Tsukuba, Japan, in 2008. He is currently an Associate Professor in the Department of Innovative Electrical and Electronic Engineering, National Institute of Technology (KOSEN), Oyama College, Oyama, Japan. His research interests include the design of high-speed interfaces, digital signal processing and sensor communication systems and their applications. Dr. Iijima received the Kenneth C. Smith Early Career Award in Microelectronics from the IEEE Computer Society Technical Committee on Multiple-Valued Logic in 2019. He served as a Program Co-Chair for IEEE International Symposium on Multiple-Valued Logic in 2023. He is a member of IEEE and IEEJ.